JACS
JOURNAL OF THE AMERICAN CHEMICAL SOCIETY
Article
pubs.acs.org/JACS

In Operando X-ray Diffraction and Transmission X-ray Microscopy of Lithium Sulfur Batteries

Johanna Nelson,[†,‡,⊥] Sumohan Misra,[†,⊥] Yuan Yang,[§,⊥] Ariel Jackson,[§] Yijin Liu,[†] Hailiang Wang,[∥] Hongjie Dai,[∥] Joy C. Andrews,[†] Yi Cui,*[,‡,§] and Michael F. Toney*[,†,‡]

[†]Stanford Synchrotron Radiation Lightsource, and [‡]Stanford Institute for Materials and Energy Science, SLAC National Accelerator Laboratory, 2575 Sand Hill Road, Menlo Park, California 94025, United States

[§]Department of Materials Science and Engineering, and [∥]Department of Chemistry, Stanford University, Stanford, California 94305, United States

Supporting Information

ABSTRACT: Rechargeable lithium−sulfur (Li−S) batteries hold great potential for high-performance energy storage systems because they have a high theoretical specific energy, low cost, and are eco-friendly. However, the structural and morphological changes during electrochemical reactions are still not well understood. In this Article, these changes in Li−S batteries are studied in operando by X-ray diffraction and transmission X-ray microscopy. We show recrystallization of sulfur by the end of the charge cycle is dependent on the preparation technique of the sulfur cathode. On the other hand, it was found that crystalline Li_2S does not form at the end of discharge for all sulfur cathodes studied. Furthermore, during cycling the bulk of soluble polysulfides remains trapped within the cathode matrix. Our results differ from previous ex situ results. This highlights the importance of in operando studies and suggests possible strategies to improve cycle life.

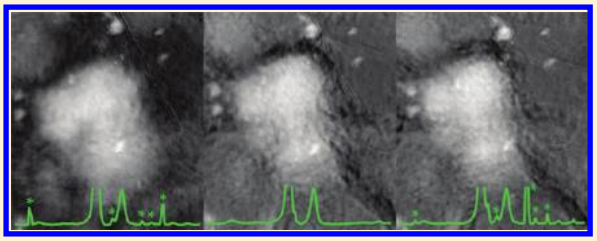

INTRODUCTION

With the ever increasing demand to move the world's energy landscape away from fossil fuels and toward clean, renewable energy, dramatic improvements in energy storage devices are essential. Sulfur is an attractive cathode material for rechargeable batteries due to its high theoretical specific capacity for a full cell (1673 mA h g^{-1}), and thus high energy density (2600 W h kg^{-1}), as compared to current state-of-the-art cathode materials based on oxides and phosphates.[1,2] Furthermore, sulfur is earth abundant, inexpensive, and nontoxic. Although recent work has demonstrated improved performance in Li-metal sulfur batteries and the feasibility of Li-ion cells using Li_2S as the cathode material,[3,4] a number of issues continue to hinder the realization of these batteries for commercial use.

The two primary obstacles are the solubility of long chain lithium polysulfides, Li_2S_x ($8 \leq x \leq 4$), formed in the early stages of the discharge cycle and the pulverization of the cathode due to volume expansion during discharge.[5] Dissolved polysulfide anions are known to diffuse through the separator to the anode creating parasitic reactions with the lithium metal resulting in the loss of active material, corrosion of the lithium anode, shuttling of polysulfides, and self-discharge.[6] Additionally, polysulfides that are not lost to the negative electrode are typically thought to reform as an insulating layer of Li_2S, which is no longer in direct contact with the electrically conductive additive, typically carbon. Efforts to improve these batteries have included the development of new electrolyte additives,[7] gelatin binders,[8] electrode coating,[9,10] novel electrolytes,[11−15] and complex sulfur/carbon morphologies.[16−24]

To guide the design of a better sulfur electrode, a more complete understanding of the reaction mechanism is needed. However, previous X-ray studies of Li−S batteries have been restricted to ex situ XRD.[25] This Article describes the use of both in operando X-ray diffraction (XRD) and in operando transmission X-ray microscopy (TXM) to study the structural and morphological changes in Li−S battery cells during operation. Such in operando studies are essential because the same battery is studied throughout the full electrochemical cycle without the addition of artifacts from post treatments.

Previously reported ex situ XRD typically shows the formation of crystalline Li_2S by the end of the discharge and no oxidation to crystalline sulfur by the end of the charge cycle.[10,11,14,26−28] Two outliers to these results are the work done by Wang et al. using gelatin as a binder, where elemental sulfur diffraction peaks reappeared after a full charge, even after 50 cycles,[8] and the work by Elazari et al. studying Li−S batteries from Sion Power Inc., which used electron diffraction to show that crystalline sulfur remained after full discharge in cells cycled fewer than 10 times and Li_2S was only evident in discharged cells cycled more than 10 times.[29]

Ex situ tomographic imaging has been used previously to visualize the 3D microstructure of a porous graphite electrode[30] as well as the 3D nanostructure and chemical distribution on a partially reduced NiO electrode material.[31] However, only a handful of in operando microscopy techniques, including TXM[32]

Received: January 9, 2012
Published: March 20, 2012

   dx.doi.org/10.1021/ja2121926 | J. Am. Chem. Soc. 2012, 134, 6337−6343

and transmission electron microscopy (TEM),[33] have been demonstrated on battery cells. Moreover, published reports on imaging of Li−S batteries have been limited to ex situ TEM, atomic force microscopy (AFM), and scanning electron microscopy (SEM),[7−11,26−29] where cycled cells are disassembled and the electrolyte washed away. SEM studies have shown the dissolution of most or all of the visible solid sulfur particles into polysulfides by the end of the first plateau region of the first discharge cycle and the formation of insoluble Li−S species on the cathode by the end of the first discharge cycle, often as films that are no longer favorably intermixed with the conductive carbon.[26−28] AFM studies of tomography, friction, and surface conductivity are in agreement with the SEM findings and show a continued decrease in surface conductivity of the cathode as the cycle number increases.[29]

Using synchrotron-based, in operando XRD, we measured diffraction patterns in real time and found that the recrystallization of sulfur is strongly dependent on the cathode preparation technique. Conversely, crystalline Li_2S never forms at the end of discharge for all cathodes studied, which is counter to published ex situ XRD results. Furthermore, with the use of in operando TXM, we found that the bulk of soluble polysulfides remain trapped within the carbon, although ex situ SEM studies on similarly prepared sulfur cathodes suggest a complete or significant loss of soluble polysulfides to the electrolyte. Both our XRD and TXM results are significantly different from previous ex situ findings and demonstrate the importance of in operando studies.

EXPERIMENTAL SECTION

Li−S in Operando Cell Construction and Electrochemistry. X-ray transparent in operando battery pouch cells were designed for both XRD and TXM. The cells are composed of a lithium metal anode, a Celgard separator soaked in an electrolyte of (1.0 M) lithium bis(trifluoromethanesulfonyl)imide (LiTFSI) in 1,3-dioxolane and 1,2-dimethoxyethane (volume ratio 1:1), and a cathode of micrometer-sized sulfur (37.5 wt %; Sigma-Aldrich), Super P carbon black (42.5 wt %; Timcal Graphite & Carbon), and Kynar PVDF binder (20 wt %; Arkema Inc.). To prepare the electrode, sulfur particles and Super P (1:1 by weight) are ball milled 10 min, and then heated to 155 °C. After being cooled, the composite is mixed with PVDF binder (20 wt %) and additional Super P (5 wt %) and ball milled another 10 min before being dispersed in *N*-methyl-2-pyrrolidone to make a slurry, which is loaded onto an aluminum current collector. The cells are assembled inside an argon-filled glovebox and heat-sealed in 0.11 mm thick polyester pouches (Kapak Co.) with aluminum and copper current collectors for cathode and anode electrodes, respectively. The cells for both techniques were identical, except TXM cells were approximately one-half the size to be compatible with the stricter sample size restrictions.

The cells were cycled at constant current, with a charge rate of C/8, unless otherwise noted, assuming a theoretical capacity of 1673 mA h g^{-1} with a MTI eight-channel battery analyzer (0.002−1 mA). The cycling current for a C/8 charge rate is calculated such that the duration for full discharge/charge is theoretically 8 h. The voltage range was 2.60−1.55 V vs Li/Li^+.

In Operando X-ray Diffraction. XRD measurements were recorded in operando at 12.74 keV at beamline 11-3 at the Stanford Synchrotron Radiation Lightsource (SSRL). The diffracted intensities were recorded on a 2D Mar345 image plate detector (Marresearch GmbH) with 150 × 150 μm^2 pixels. Measurements were done in transmission with a detector distance 145 mm from the sample center. The incident beam on the sample was approximately 50 × 50 μm^2. Figure S1 shows the layout of the experiment. For in operando measurements, diffraction intensities were collected in 5 min intervals with 210 s exposure time. Data were internally calibrated using the aluminum diffraction peaks and analyzed with Area Diffraction Machine.[34] WinPlotr,[35] which is part of the FullProf Suite Program (1.10), was used for background subtraction.[36]

In Operando Transmission X-ray Microscopy. TXM was performed in operando using a full-field Xradia microscope at SSRL beamline 6-2c. The microscope is optimized to operate between ∼5 and 14 keV. For the lithium sulfur batteries, micrographs were taken at 6 keV, an energy that both optimizes the sulfur contrast and the efficiency of the objective lens. The spatial resolution provided by the instrument is as fine as 30 nm with a field of view typically around 15−30 μm. For the in operando microscopy presented here, a total of five sample positions were imaged at approximately 5 min intervals with a camera binning of 2. The raster scanning capability of the microscope was used to image regions of ∼40 × 40 μm^2. Additional details about the microscope are found in papers by Andrews et al.,[37] Liu et al.,[38] and Meirer et al.[31]

To maintain good electrical contact inside the in operando pouch cells during imaging, moderate pressure is applied using two parallel aluminum plates shown in Figure 1, where the pressure can be controlled by tightening four screws that hold the plates together. Samples are imaged through a horizontal through-hole, which is designed with a cut-away to permit X-rays to pass unobstructed even at large imaging angles. This allows for the capability of future in situ 3D imaging, where 2D images from many viewing angles are required. Finally, there is an additional through-hole, which is not occluded by the sample and allows reference images to be taken. Reference images were taken approximately every 25 min and were used to remove imaging artifacts due to imperfections in the X-ray beam and detector system. Micrographs were processed using TXM Wizard.[39,40] Analysis included reference correction, repeated exposure averaging, mosaic stitching, and alignment of sequential images.

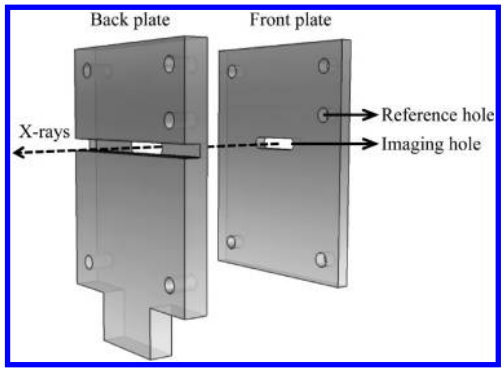

Figure 1. In operando sample holder plates for TXM. The pouch cell is placed between the plates, and moderate pressure is applied with four screws. The aluminum plates allow X-ray imaging through the sample imaging hole as well as the unobstructed reference hole while maintaining enough pressure for normal operation of the cell. The back plate has a cut-away to allow for future 3D imaging by tomography, which requires images to be taken through a large angular range.

RESULTS AND DISCUSSION

In Operando X-ray Diffraction. Figure 2 shows the in operando XRD results on a Li−S cell during the first galvanostatic electrochemical cycle, as a function of specific capacity. The XRD pattern at the start of the discharge cycle is presented in Figure 2a with the diffraction peaks associated with crystalline S (Q = 1.09, 1.63, 1.82, 1.89, 1.96, 3.27, and 3.65 $Å^{-1}$; JCPDS no. 01-073-5065), Li (Q = 2.53 and 5.07 $Å^{-1}$; JCPDS no. 01-001-1131), and Al (Q = 2.69, 3.10, 4.39, 5.15, and 5.37 $Å^{-1}$; JCPDS no. 01-004-0787) labeled. All unlabeled peaks are associated with either the polyester pouch or the polymer separator. Figure 2b contains a magnified view of the

dx.doi.org/10.1021/ja2121926 | J. Am. Chem. Soc. 2012, 134, 6337−6343

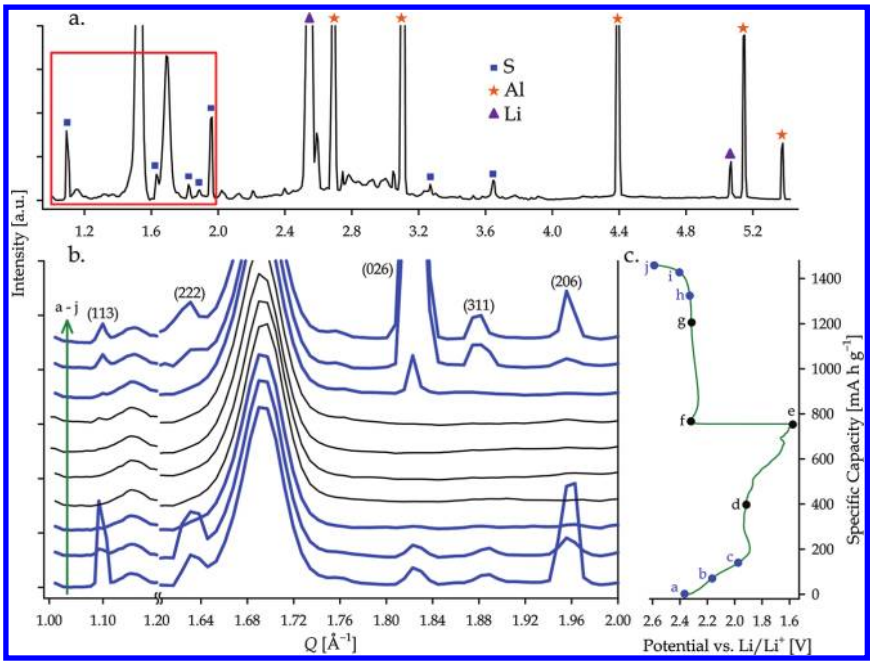

Figure 2. In operando XRD patterns of a Li−S cell cycled at C/8 and with a cathode prepared as a sulfur/Super P composite: (a) XRD pattern at the start of the discharge cycle; (b) XRD patterns for the region of Q-space marked by the red box in (a) for points a−j labeled in (c) the corresponding electrochemical plot. The XRD patterns show the reappearance of sulfur diffraction peaks at the end of the first charge cycle. Sulfur peaks in (b) are labeled with their Miller indices. Unlabeled peaks are from the polyester pouch and separator. XRD patterns that are blue include sulfur peaks. The total discharge capacity is 755 mA h g^{-1}, and the total charge capacity is 707 mA h g^{-1}.

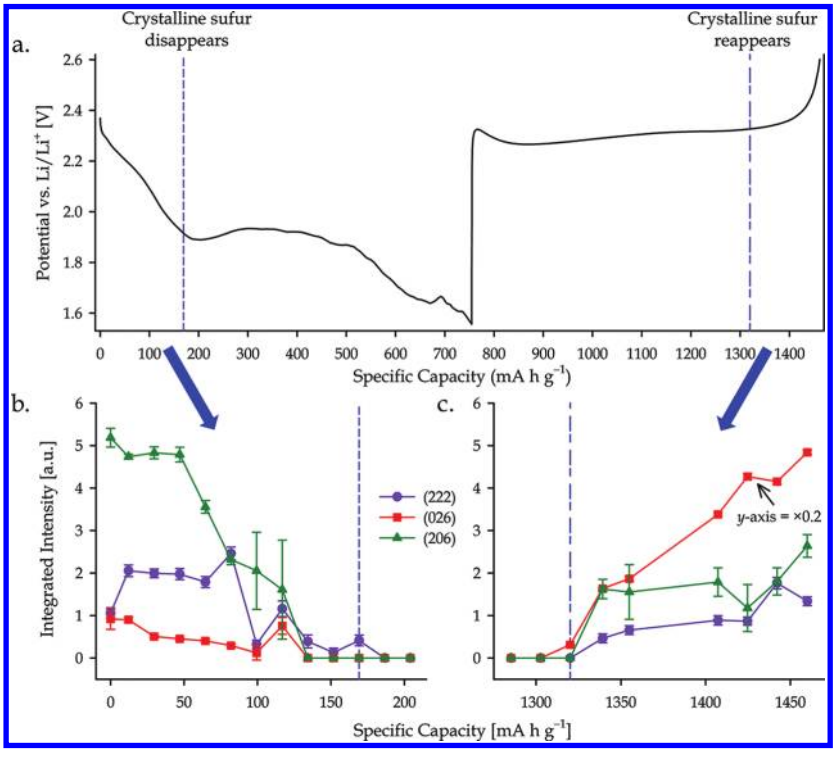

Figure 3. Integrated diffraction intensities of sulfur peaks for a Li−S cell cycled at C/8 and with a cathode prepared as a sulfur/Super P composite: (a) electrochemical plot showing the first cycle of the Li−S cell; (b and c) integrated intensity plots for (222), (026) ,and (206) Bragg peaks, which show the disappearance of crystalline sulfur by the end of the first discharge plateau and its reappearance by the end of the charge cycle. The blue arrows indicate the specific capacity regions over which the integrated intensities are plotted. The dashed lines emphasize where sulfur peaks disappear and reappear. The total discharge capacity is 755 mA h g^{-1}, and the total charge capacity is 707 mA h g^{-1}. Error bars on the integrated intensities were determined using Levenberg−Marquardt minimization.

section of Q-space indicated by a red box in Figure 2a, as sulfur is reduced in accordance with the electrochemical plot shown in Figure 2c. During reduction, the sulfur peaks decrease in intensity and disappear completely before the end of the first

dx.doi.org/10.1021/ja2121926 | J. Am. Chem. Soc. 2012, 134, 6337−6343

discharge plateau, indicating that all of the crystalline sulfur is reacting with lithium ions. During the charging cycle, sulfur peaks reappear toward the end of the cycle, indicating that polysulfides have oxidized to crystalline sulfur. This phase evolution is consistent for a cell of the same electrode morphology cycled at $C/20$ (Figure S2), suggesting that cycle rate does not change the phase behavior. These results are contrary to most previous ex situ results, which report the active material remains as polysulfides at the end of the charge cycle.[11,26,28] Nevertheless, other factors such as current density or type of salt and solvent used, which can modify the phase evolution, were not explored.

To more clearly establish this behavior, the integrated intensities of the sulfur (222), (026), and (206) Bragg peaks are plotted in Figure 3 as a function of specific capacity. To calculate the integrated intensities, the peaks were fit with pseudo-Voigt functions. The relative integrated intensities of the three peaks of the pristine sulfur are different from those at the end of the charge cycle, which indicates a possible reorientation of the sulfur particles upon recrystallization. Similar changes in relative sulfur peak intensity are also seen in the cell cycled at $C/20$ (Figure S2). This prohibits any estimation of the amount of crystalline sulfur present after the first charge cycle.

Notably, Figure 2 shows no crystalline Li_2S peak at 1.90 $Å^{-1}$ (JCPDS no. 01-089-1730) at the end of discharge cycle in contrast to previous ex situ reports.[8,10,11,14,26−28] Nevertheless, according to the electrochemical cycle, it is likely that amorphous Li_2S is forming; however, its existence in an amorphous state was not confirmed in this study. The presence of an amorphous rather than the crystalline form could have an influence on the insulating nature of the Li_2S on the cathode.

To explore whether or not the reappearance of crystalline sulfur and the lack of crystalline Li_2S are direct consequences of the preparation method of the sulfur/Super P composite electrode or the in operando nature of the experiment, two alternative preparation methods were investigated at a rate of $C/10$. The first alternative was prepared as a slurry of micrometer-sized sulfur particles mixed with Super P carbon black and PVDF binder (see the Supporting Information for preparation details). The second was graphene-wrapped polyethylene glycol-coated sulfur particles (see Wang et al. for preparation details).[22] SEM micrographs with corresponding energy-dispersive X-ray spectroscopy (EDS) sulfur maps are given in Figure S3 for all three preparation methods. For both of these alternative methods, diffraction peaks of Li_2S after discharge and elemental sulfur after charge were not visible (Figures S4 and S5). It follows that the reappearance of crystalline sulfur is strongly dependent on the cathode morphology dictated by the preparation technique. However, all three preparation methods studied did not form crystalline Li_2S during the discharge cycle.

To further test if the absence of crystalline Li_2S is due to the cathode preparation method or the in operando nature of the experiment, ex situ XRD data were recorded on a discharged Li−S cell with sulfur/Super P composite electrode. Figure 4 shows ex situ XRD on the electrode with the Li_2S peaks at 1.9 and 2.2 $Å^{-1}$ (JCPDS no. 01-089-1730) labeled. This suggests that amorphous Li_2S is formed during discharge, and only when a discharged cell is allowed to rest does crystalline Li_2S form. Further investigations are required to determine the time window in which crystalline Li_2S forms and to verify the existence of amorphous Li_2S. Nevertheless, these results demonstrate that in operando XRD is necessary for proper characterization of the Li−S

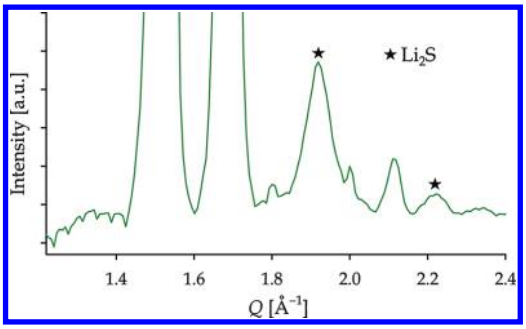

Figure 4. Ex situ XRD on an electrode discharge to 1043 mA h g^{-1}. Li_2S peaks at 1.9 and 2.2 $Å^{-1}$ (JCPDS no. 01-089-1730) are labeled. Unlabeled peaks are from the polyester pouch.

battery crystalline structure and that the previously observed Li_2S may be an artifact of ex situ XRD.

In Operando Transmission X-ray Microscopy. Figure 5a shows a TXM micrograph of a pristine Li−S cell with a ∼10 μm sized sulfur/Super P composite particle. Because of the low absorption of carbon as compared to sulfur at 6 keV, the contrast between the sulfur/Super P composite particles and the background is high. Furthermore, the brighter the particle, the more sulfur it contains throughout its thickness. This heterogeneous mixing of sulfur and Super P carbon into micrometer-sized particles is typical throughout the electrode as seen in Figure S6a, which is a mosaic comprised of 2 × 2 TXM micrographs, in which the bottom left tile contains the particle from Figure 5a.

The nine micrographs shown in Figure 5 are a selection from those recorded every 5 min throughout the first electrochemical cycle of the pouch cell. The frame labels correspond to the points along the cycle in Figure 6b. Although subtle, the majority of the morphological changes occur in images a−c, corresponding to the first discharge plateau where elemental sulfur reduces to high-order Li polysulfides. During this plateau, the particle expands slightly, but simultaneously loses some active material through the dissolution of polysulfides, creating a slightly smaller particle with a more porous appearance and an increase in the X-ray absorption of the background. The green outline around the particle in (a) is replicated in (c) to show the overall decrease in particle size and increased porosity. Yellow arrows have been added to draw attention to a smaller particle that is expanding between (a) and (b). These micrographs suggest that, although some polysulfides diffuse into the electrolyte, the majority of the active material is not lost. Considering that the cycle life of these cells remains poor (Figure S7), even a small amount of polysulfides diffusing into the electrolyte appears to lead to substantial capacity fading.

The loss of polysulfides to the electrolyte can be monitored by calculating the contrast between particles and background throughout the cycle. Figure 6a plots the change in average contrast of sulfur/Super P composite particles with respect to specific capacity for five different regions across the electrode.[41] The average contrast drops dramatically in the first discharge plateau and then remains relatively flat through the remaining discharge cycle and subsequent charge cycle, which is consistent with the morphological changes visible in Figure 5.

According to the previously described in operando XRD results, and because the morphological changes are consistent throughout mosaic images taken at five regions across the electrode (see, for example, Figures S6 and S8), sulfur is reduced, but the resulting polysulfides are primarily trapped by the SuperP carbon matrix. Furthermore, because the particle

dx.doi.org/10.1021/ja2121926 | J. Am. Chem. Soc. 2012, 134, 6337−6343

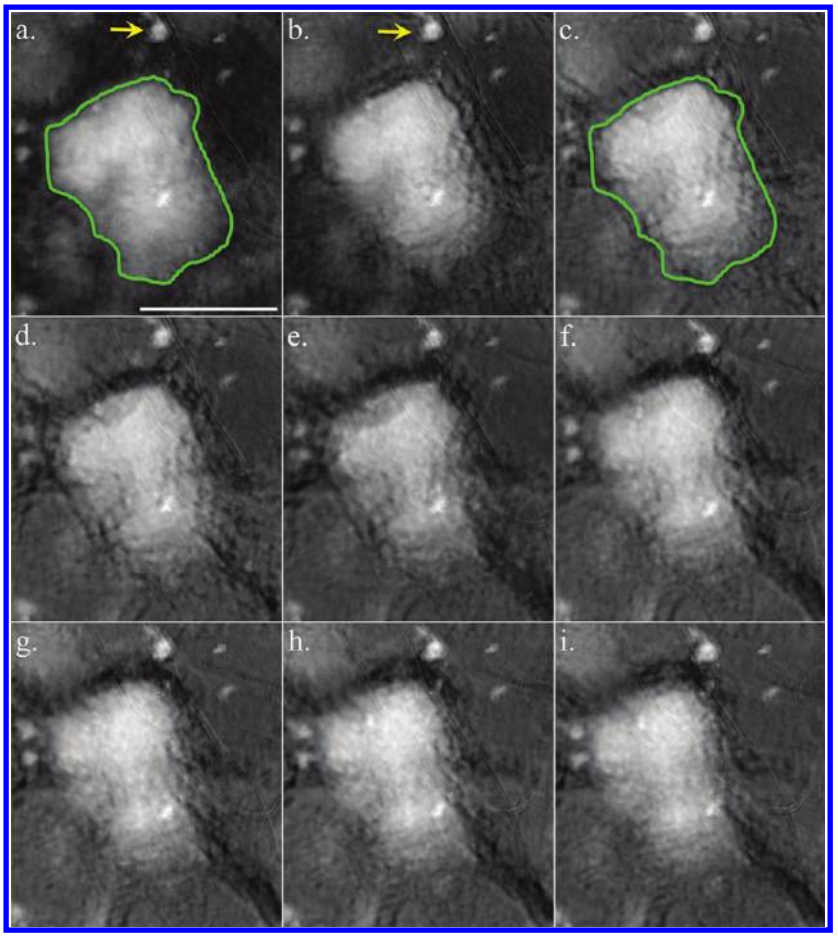

Figure 5. In operando TXM micrographs of a sulfur/Super P composite particle during operation, where the letters correspond to points along the electrochemical cycle labeled a–i in Figure 6. The majority of morphological changes occur between images a and c, corresponding to the first plateau of the discharge. Micrographs were taken at 6 keV and are an average of three 5 s exposures recorded approximately every 5 min with a CCD binning of 2. The green outline around the particle in (a) is replicated in (c) to show the overall decrease in particle size and increased porosity. The yellow arrows show a small particle that expands between (a) and (b). The scalebar is 10 μm.

does not grow in size during the second discharge plateau (d–f) and there is no formation of new particles, the material that is lost does not solidify onto the existing particle or form new particles. Instead, the background remains more absorbing, and isolated regions of low sulfur density form, which are visible as darker, X-ray transparent regions. This suggests that the insoluble polysulfides form thin films, which is in agreement with previous ex situ results. A movie showing the entire cycle of the particle from Figure 5 is available in the Supporting Information (movie S1) as well as a second movie on an additional particle (movie S2).

Ex Situ Scanning Electron Microscopy. To confirm the interpretation of the in operando TXM results, ex situ SEM images were recorded on sulfur/Super P composite electrodes. Figure 7 shows ex situ SEM micrographs and corresponding sulfur EDS maps of sulfur/Super P composite cathodes in (a,b) pristine, (c,d) discharged to the end of the first plateau, and (e,f) fully discharged states. The SEM micrograph of the pristine electrode (a) and EDS sulfur map (b) of the same area indicate a correlation between particles and increased sulfur concentration. The concentration of sulfur in ~5–10 μm-sized particles agrees with the heterogeneity visible in the TXM images.

The particles visible on the electrode discharged to the end of the first plateau (c) are approximately the same size as those sulfur-rich ones visible in the pristine electrode (a), although the sulfur EDS signal is very low for this partially discharged electrode (d). This negligible change in average particle size agrees with the conclusion that most of the polysulfides that make up the particles are not lost to the electrolyte; however, the lack of sulfur EDS signal suggests that the polysulfides trapped in the carbon matrix are washed away during the SEM preparation. After discharge (e), the electrode is coated with a film of insoluble lithium sulfur species, and the EDS map (f) shows a uniform distribution of sulfur. This uniform film-like plating of insoluble lithium sulfide species is consistent with TXM results, as it does not produce an increase in particle size, form new particles, or improve the particle-to-background contrast.

Higher magnification SEM micrographs are shown in Figure S9 to demonstrate local surface details. These micrographs also suggest that, although the average size of the large sulfur/Super P composite particles is unchanged (b) after the first discharge plateau, the trapped polysulfides are washed away during the SEM preparation. Furthermore, the lithium sulfide film coating the electrode (c) after discharge has some regular texture.

The in operando TXM micrographs show sulfur species remain as composite particles throughout the electrochemical cycle. In contrast, for an electrode discharged to the end of the first plateau, high magnification SEM micrographs exhibit no visible sulfur, and the EDS map of the same electrode shows very low sulfur content. These results highlight the importance of in operando

dx.doi.org/10.1021/ja2121926 | J. Am. Chem. Soc. 2012, 134, 6337–6343

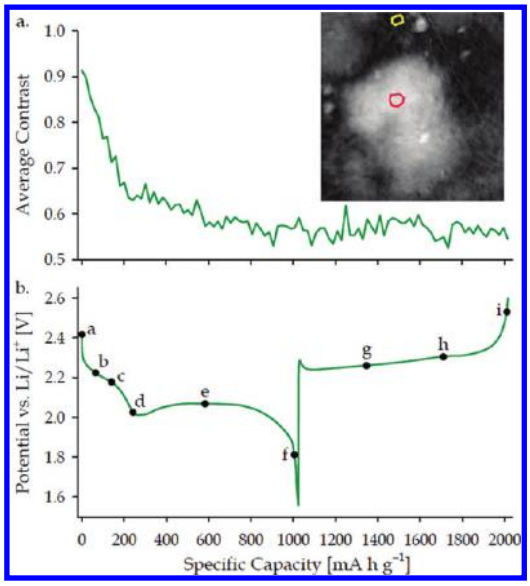

Figure 6. (a) Change in average contrast versus specific capacity in TXM micrographs of a Li−S battery cycled at *C*/8 and (b) the cell potential. Letters a−i correspond to the capacities at which the micrographs shown in Figure 5 were recorded. The average contrast was calculated between the average pixel in a small region within a particle and a similarly sized region of the background averaged for five different particles, each with two different chosen particle and background regions. The inset gives an example of a particle region in red with the background region in yellow.

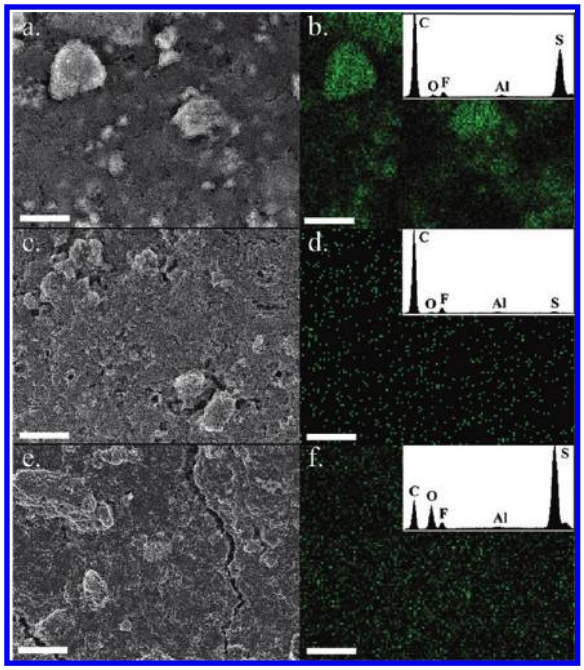

Figure 7. Ex situ SEM micrographs and corresponding EDS sulfur maps of the sulfur/Super P composite cathode: (a,b) uncycled, (c,d) after the first discharge plateau, and (e,f) fully discharged. The scalebars are 10 μm.

characterization of Li−S batteries to eliminate artifacts introduced during SEM post-treatments.

Using in operando TXM, we have shown that the bulk of the soluble polysulfides are trapped and not lost to the electrolyte, which demonstrates the partial efficacy of this morphology for reducing capacity fade. Nevertheless, the polysulfides that do escape solidify as an insulating film, and this loss results in the observed capacity fade. To completely trap the soluble polysulfides and thereby improve the Li−S battery lifetime, a more intricate sulfur/carbon electrode morphology, such as sulfur-filled mesoporous carbon, is needed.[16,18,21] Future in operando TXM studies will include verifying the trapping capability of electrodes utilizing such complex sulfur/carbon morphologies. Additionally, hard X-ray TXM is not surface sensitive; thus the entire sulfur contained in a ~10 μm particle was monitored. This characteristic allows the possibility of future 3D in situ X-ray imaging to accurately measure volume and density changes of the sulfur particles.

SUMMARY AND CONCLUSION

By performing XRD on Li−S cells during operation, the same cell could be monitored in real time throughout its entire first cycle. The recrystallization of sulfur after the charge cycle was found to only occur with the sulfur/Super P composite electrodes. In operando TXM allows individual particles to be tracked in real time throughout the electrochemical cycle. Contrary to previous ex situ studies, the sulfur/Super P composite particles were not found to dissolve significantly during the first discharge plateau. This trapping of the polysulfides may promote the crystallization of sulfur by the end of the charge cycle. Nevertheless, even the small amount of polysulfides lost to the electrolyte appears to have a significant impact on the cycle life. Finally, in operando XRD showed no formation of crystalline Li_2S during the discharge cycle, which contradicts previously reported ex situ studies of similar Li−S batteries.

The results shown here highlight the need for in operando characterization of Li−S batteries. Such experiments reveal new insights by making observations during the entire electrochemical cycle and by eliminating post treatments. Our results suggest that more complete encapsulation of the sulfur will result in a Li−S battery with a longer lifetime.

ASSOCIATED CONTENT

Supporting Information

Discussion of in operando XRD at rate of *C*/20, description of micrometer-sized sulfur particle preparation, SEM with EDS detector experimental information, ex situ XRD experimental information, image of in operando XRD setup, in operando XRD of sulfur/Super P composite electrode cycled at *C*/20, SEM and EDS images of the three cathode preparation methods, XRD of the alternative cathode preparation methods, in operando TXM mosaics, plot of cycle life of Li−S cell with sulfur/Super P composite cathode, high magnification ex situ SEM micrographs, and two movies of in operando TXM. This material is available free of charge via the Internet at http://pubs.acs.org.

AUTHOR INFORMATION

Corresponding Author

mftoney@slac.stanford.edu; yicui@stanford.edu

Author Contributions

⊥These authors contributed equally to this work.

Notes

The authors declare no competing financial interest.

ACKNOWLEDGMENTS

Portions of this research were carried out at the Stanford Synchrotron Radiation Lightsource, a national user facility operated by

Stanford University on behalf of the U.S. Department of Energy, Office of Basic Energy Sciences. This work is supported by the Department of Energy, Laboratory Direct Research and Development funding, under contracts DE-AC02-76SF00515 (J.N., J.C.A., M.F.T.) and DE-AC02-76SF00515 (Y.C.). Y.Y. acknowledges support from a Stanford Graduate Fellowship, and A.J. acknowledges support from the Department of Defense (DoD) through the National Defense Science & Engineering Graduate Fellowship (NDSEG) Program.

REFERENCES

(1) Whittingham, M. S. *Chem. Rev.* **2004**, *104*, 4271.
(2) Ellis, B. L.; Lee, K. T.; Nazar, L. F. *Chem. Mater.* **2010**, *22*, 691.
(3) Hassoun, J.; Sun, Y.-K.; Scrosati, B. *J. Power Sources* **2011**, *196*, 343.
(4) Yang, Y.; McDowell, M. T.; Jackson, A.; Cha, J. J.; Hong, S. S.; Cu, Y. *Nano Lett.* **2010**, *10*, 1486.
(5) Yang, Y.; Yu, G.; Cha, J. J.; Wu, H.; Vosgueritchian, M.; Yao, Y.; Bao, Z.; Cui, Y. *ACS Nano* **2011**, *5*, 9187.
(6) Mikhaylik, Y. V.; Akridge, J. R. *J. Electrochem. Soc.* **2004**, *151*, A1969.
(7) Choi, J.-W.; Cheruvally, G.; Kim, D.-S.; Ahn, J.-H.; Kim, K.-W.; Ahn, H.-J. *J. Power Sources* **2008**, *183*, 441.
(8) Wang, Y.; Huang, Y.; Wang, W.; Huang, C.; Yu, Z.; Zhang, H. *Electrochim. Acta* **2009**, *54*, 4062.
(9) Lee, Y. M.; Choi, N.-S.; Park, J. H.; Park, J.-K. *J. Power Sources* **2003**, *119*−*121*, 964.
(10) Choi, Y.-J.; Chung, Y.-D.; Baek, C.-Y.; Kim, K.-W.; Ahn, H.-J.; Ahn, J.-H. *J. Power Sources* **2008**, *184*, 548.
(11) Ryu, H.-S.; Ahn, H.-J.; Kim, K.-W.; Ahn, J.-H.; Lee, J.-Y. *J. Power Sources* **2006**, *153*, 360.
(12) Yuan, L. X.; Feng, J. K.; Ai, X. P.; Cao, Y. L.; Chen, S. L.; Yang, H. X. *Electrochem. Commun.* **2006**, *8*, 610.
(13) Choi, J.-W.; Kim, J.-K.; Cheruvally, G.; Ahn, J.-H.; Ahn, H.-J.; Kim, K.-W. *Electrochim. Acta* **2007**, *52*, 2075.
(14) Jeong, S. S.; Lin, Y. T.; Choi, Y. T.; Cho, G. B.; Kim, K. W.; Ahn, H. J.; Cho, K. K. *J. Power Sources* **2007**, *174*, 745.
(15) Shin, J. H.; Cairns, E. J. *J. Power Sources* **2008**, *177*, 537.
(16) Ji, X.; Lee, K. T.; Nazar, L. F. *Nat. Mater.* **2009**, *8*, 500.
(17) Lai, C.; Gao, X. P.; Zhang, B.; Yan, T. Y.; Zhou, Z. *J. Phys. Chem. C* **2009**, *113*, 4712.
(18) Liang, C.; Dudney, N. J.; Howe, J. Y. *Chem. Mater.* **2009**, *21*, 4724.
(19) Jayaprakash, N.; Shen, J.; Moganty, S. S.; Corona, A.; Archer, L. A. *Angew. Chem., Int. Ed.* **2011**, *50*, 5904.
(20) Cao, Y.; Li, X.; Aksay, I. A.; Lemmon, J.; Nie, Z.; Yang, Z.; Liu, J. *Phys. Chem. Chem. Phys.* **2011**, *13*, 7660.
(21) Li, X.; Cao, Y.; Qi, W.; Saraf, L. V.; Xiao, J.; Nie, Z.; Mietek, J.; Zhang, J.-G.; Schwenzer, B.; Liu, J. *J. Mater. Chem.* **2011**, *21*, 16603.
(22) Wang, H.; Yang, Y.; Liang, Y.; Robinson, J. T.; Li, Y.; Jackson, A.; Cui, Y.; Dai, H. *Nano Lett.* **2011**, *11*, 2644.
(23) Wang, J.-Z.; Lu, L.; Choucair, M.; Stride, J. A.; Xu, X.; Liu, H.-K. *J. Power Sources* **2011**, *196*, 7030.
(24) Zheng, G.; Yang, Y.; Cha, J. J.; Hong, S. S.; Cui, Y. *Nano Lett.* **2011**, *11*, 10.
(25) An in situ, but not in operando, XRD was performed on a Li_2S half cell with composite gel polymer electrolyte, where electrochemical cycling was interrupted at various stages to collect XRD data.[3] We have not included this experiment in our discussion.
(26) Cheon, S.-E.; Ko, K.-S.; Cho, J.-H.; Kim, S.-W.; Chin, E.-Y.; Kim, H.-T. *J. Electrochem. Soc.* **2003**, *150*, A796.
(27) Ryu, H.-S.; Guo, Z.; Ahn, H.-J.; Cho, G. B.; Liu, H. *J. Power Sources* **2009**, *189*, 1179.
(28) Yuan, L.; Qiu, X.; Chen, L.; Zhu, W. *J. Power Sources* **2009**, *189*, 127.
(29) Elazari, R.; Salitra, G.; Talyosef, Y.; Grinblat, J.; Scordilis-Kelley, C.; Xiao, A.; Affinito, J.; Aurbach, D. *J. Electrochem. Soc.* **2010**, *157*, A1131.
(30) Shearing, P. R.; Howard, L. E.; Jørgensen, P. S.; Brandon, N. P.; Harris, S. J. *Electrochem. Commun.* **2010**, *12*, 374.
(31) Meirer, F.; Cabana, J.; Liu, Y.; Mehta, A.; Andrews, J. C.; Pianetta, P. *J. Synchrotron Radiat.* **2011**, *18*, 773.
(32) Chao, S.-C.; Yen, Y.-C.; Song, Y.-F.; Chen, Y.-M.; Wu, H.-C.; Wu, N.-L. *Electrochem. Commun.* **2010**, *12*, 234.
(33) Huang, J. Y.; Zhong, L.; Wang, C. M.; Sullivan, J. P.; Xu, W.; Zhang, L. Q.; Mao, S. X.; Hudak, N. S.; Liu, X. H.; Subramanian, A.; Fan, H.; Qi, L.; Kushima, A.; Li, J. *Science* **2010**, *330*, 1515.
(34) Lande, J.; Webb, S. M.; Mehta, A. *Area Diffraction Machine* 2008, http://code.google.com/p/areadiffractionmachine/.
(35) Roisnel, T.; Rodriguez-Carvajal, J. *Proc. Seventh EPDIC* **2000**, 118.
(36) Rodriguez-Carvajal, J. *Physica B* **1993**, *192*, 55.
(37) Andrews, J. C.; Almeida, E.; van der Meulen, M. C. H.; Alwood, J. S.; Lee, C.; Liu, Y.; Chen, J.; Meirer, F.; Feser, M.; Gelb, J.; Rudati, J.; Tkachuk, A.; Yun, W.; Pianetta, P. *Microsc. Microanal.* **2010**, *16*, 327.
(38) Liu, Y.; Andrews, J. C.; Wang, J.; Meirer, F.; Zhu, P.; Pianetta, P. *Opt. Express* **2011**, *19*, 540.
(39) Liu, Y.; Williams, P. *TXM Wizard* 2011, http://sourceforge.net/projects/txm-wizard/.
(40) Liu, Y.; Meirer, F.; Williams, P. A.; Wang, J.; Andrews, J. C.; Pianetta, P. *J. Synchrotron Radiat.* **2012**, *19*, 281.
(41) The contrast was defined as the difference of the average intensity in a small region within a particle and the average intensity in a similarly sized region of background divided by the sum of the two averages. The inset in Figure 6a shows an example of such a region for a particle in red with the background in yellow. To ensure consistent conclusions, the contrast was calculated for two different regions per particle.